Parametrization of the relaxation time in crystalline graphite

Ney J. Luiggi and Willians Barreto
Departamento de Física Escuela de Ciencias, Universidad de Oriente, Apartado de Correos 245, Cumaná, Venezuela
(Received 16 December 1985)

The band theory of Slonczewsky, Weiss, and McClure (SWMc) is combined with an electron-phonon interaction to determine the relaxation time in crystalline graphite as a function of the interaction parameters. The transition probability between Bloch functions, which include atomic displacements due to thermal vibration of the lattice, is evaluated. Wave functions are expanded at each atomic site, leading to a simple relationship between the electron-phonon interaction and the relaxation time. The splitting of the relaxation time parallel and perpendicular to the graphite plane is introduced through the transition probability. The Komatsu dispersion relation, for parallel and perpendicular acoustic phonons, is adjusted through experimental measurement. Relaxation times are evaluated as a function of energy for temperatures between 25 and 300 K, giving results that depend on the interaction parameters used. Both parallel and perpendicular relaxation times are of the same order of magnitude, and the parallel relaxation time agrees with the one calculated using Ono's theory.

I. INTRODUCTION

The study of the electric and magnetic properties of graphite has been the subject of much research, because these properties mix structural details of the real and reciprocal lattices, the band structure, the Fermi surface, and also dispersive processes undergone by electrons.

Graphite is a semimetal with a hexagonal lattice where the atoms are distributed in layers, with four atoms per unit cell [Figs. 1(a) and 1(b)]. The interatomic distance within a layer is smaller than the distance between layers. This introduces an important anisotropy which renders the planar properties much different from those evaluated in the direction normal to the layers.

The first Brillouin zone of this structure is hexagonal with a strong electron distribution at the edges HKH'.[1] The band structure of graphite has been studied by different methods[2,3] but when dealing with transport properties, two models have been used preferentially: the Slonczewski-Weiss-McClure (SWMc) model,[1,4] which makes use of the electron distribution at the edges of the first Brillouin zone, and the Johnson-Dresselhaus model,[5] which makes use of the whole first zone. In both cases the band structure is obtained from Bloch wave functions in which $2p_z$ orbitals of the four atoms of the base intervene to form the π bands. The Fermi level lies between these bands. The σ bands, related to other orbitals of the sp^2 hybridization of the isolated carbon atoms, are sufficiently separated from the π bands; for that reason only the π bands are considered in the study of transport coefficients.

Also, the transport coefficients referred to in the Boltzmann theory are in one way or another related to the relaxation time, which depends on the scattering processes undergone by the electrons due to impurities, lattice vibrations, or any other defects in the kind of graphite used. Each of those mechanisms has its temperature range of dominance over the others. In crystalline graphite, for $T > 50$ K, the electron scattering is due to electron-phonon interactions. The phononic modes can be separated into parallel and normal modes referred to the graphite plane.[6]

In the literature, we can see that different models for the relaxation time have been used to evaluate the transport coefficients. Wallace,[7] in an attempt to explain the electric resistivity of crystalline graphite, introduced a phenomenologic relaxation time in which the Debye tem-

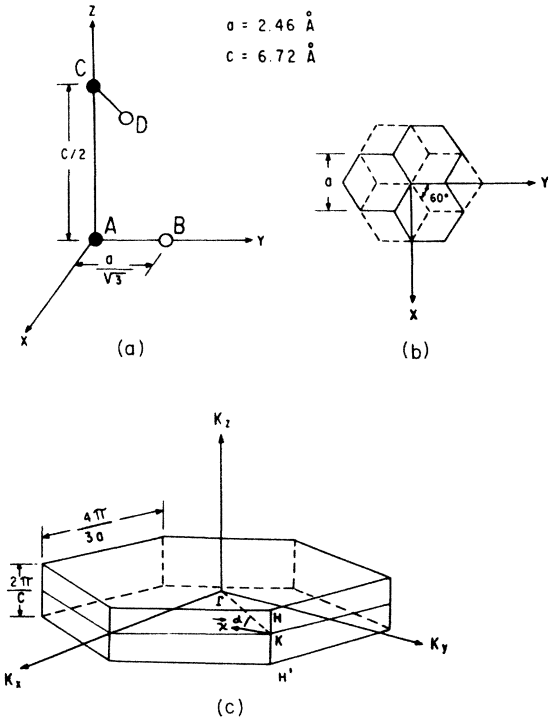

FIG. 1. (a) Atoms in the base. (b) Graphitic lattice. (c) First Brillouin zone.

perature entered into the electron-phonon interaction. Sugihara and Sato[8] and Ono and Sugihara[9] have made a more consistent theory, through the combination of the band structure and the electron-phonon interaction. In their case, they used the rigid-ion model. Although this theory is mathematically complete, its complexity obligates one to make posterior suppositions to introduce constants of adjustment that restrict its generality. Besides, the rigid-ion model restricts the type of phonons that participate in the dispersion processes. Most of the work on transport coefficients that followed[10,11] used the Ono theory as a starting point.

In this work we present a different way of checking the electron-phonon interaction in graphite. This method will be used to evaluate the planar and perpendicular relaxation times as functions of energy for different temperatures. The band structure is taken from the model of SWMc, and we will use in it the interaction parameters more frequently reported in the literature. The phonon dispersion relations are taken from experiments.[12]

II. BAND STRUCTURE AND CONSTANT-ENERGY SURFACES

In accordance with the ideas of SWMc, the band structure is obtained with a crystal wave function $|\Psi\rangle$ which is a linear combination of Bloch functions which are centered at each atom of the basis [Figs. 1(a) and 1(b)]. Each of the functions is characterized by a $2p_z$ orbital:[4]

$$|\Psi\rangle=\sum_{n=1}^{4}\lambda_n|\phi_n\rangle\ , \tag{1}$$

where

$$|\phi_1\rangle=\frac{1}{\sqrt{2}}(|\phi_A\rangle+|\phi_C\rangle),\ |\phi_2\rangle=\frac{1}{\sqrt{2}}(|\phi_A\rangle-|\phi_C\rangle)\ ,$$

$$|\phi_3\rangle=|\phi_B\rangle,\quad |\phi_4\rangle=|\phi_D\rangle\ . \tag{2}$$

$|\phi_n(n=A,B,C,D)\rangle$ designates the wave function centered at the nth atom. The selection of the basis $|\phi_n(n=1,2,3,4)\rangle$, instead of $|\phi_n(n=A,B,C,D)\rangle$, avoids certain energetic degeneration around the HKH' edge.

The $|\phi_n\rangle$ are wave functions characteristic of the tight-binding model defined by

$$|\phi_n(n=A,B,C,D)\rangle=\frac{1}{\sqrt{N}}\sum_j\exp(i\mathbf{k}\cdot\mathbf{r}_j^n)\,|\phi(\mathbf{r}-\mathbf{r}_j^n)\rangle\ , \tag{3}$$

where the summation is over the j atoms ($j=A,B,C,D$) of the N graphitic unit cells and $|\phi(\mathbf{r}-\mathbf{r}_j^n)\rangle$ is the $2p_z$ atomic orbital associated with the nth atom.

The Schrödinger equation leads to a system of equations in λ_j, such that

$$\sum_{n,j}\lambda_j(H_{nj}-ER_{nj})=0\ , \tag{4}$$

with

$$H_{nj}=\langle\phi_n|H|\phi_j\rangle$$

and

$$R_{nj}=\langle\phi_n|\phi_j\rangle\ .$$

The Hamiltonian H can be separated into a Hamiltonian H_0 associated with isolated atoms and another H' which takes into account the details of the lattice. The R_{nj} are the overlap integrals of the atomic orbitals and the H_{nj} are the interaction integrals between ϕ_n and ϕ_j. The evaluation of these integrals is rather difficult; for this reason the Hamiltonian is written in terms of the interaction parameters γ_i.

Using Hückel's approximation,[13] the secular equation can be written in the form

$$\begin{vmatrix} E_1-E & 0 & H_{13} & H_{14} \\ 0 & E_2-E & H_{23} & H_{24} \\ H_{13}^* & H_{23}^* & E_3-E & H_{34} \\ H_{14}^* & H_{24}^* & H_{34}^* & E_3-E \end{vmatrix}=0\ , \tag{5}$$

where

$$\begin{aligned}
H_{13}&=2^{-1/2}S_{AB}(2\gamma_4\cos\Theta-\gamma_0)\ ,\\
H_{14}&=2^{-1/2}S_{AB}^*(2\gamma_4\cos\Theta-\gamma_0)\ ,\\
H_{23}&=-2^{-1/2}S_{AB}(2\gamma_4\cos\Theta-\gamma_0)\ ,\\
H_{24}&=2^{-1/2}S_{AB}^*(2\gamma_4\cos\Theta-\gamma_0)\ ,\\
H_{34}&=2\cos(\Theta/2)S_{AB}\ ,\\
E_1&=\Delta+2\gamma_1\cos\Theta+2\gamma_5\cos^2\Theta\ ,\\
E_2&=\Delta-2\gamma_1\cos\Theta+2\gamma_5\cos^2\Theta\ ,\\
E_3&=2\gamma_2\cos^2\Theta\ ,\\
S_{AB}&=S_{AB}^R+iS_{AB}^I\ ,\\
S_{AB}^R&=3^{1/2}\sin(\tfrac{1}{2}U)\cos(\tfrac{1}{2}\tilde{N})\\
&\quad-\cos(\tfrac{1}{2}\tilde{N})\cos(\tfrac{1}{2}U)+\cos(\tilde{N})\ ,\\
S_{AB}^I&=3^{1/2}\sin(\tfrac{1}{2}U)\sin(\tfrac{1}{2}\tilde{N})\\
&\quad-\sin(\tfrac{1}{2}\tilde{N})\cos(\tfrac{1}{2}U)-\sin(\tilde{N})\ ,
\end{aligned} \tag{6}$$

with

$$U=a\chi\cos\alpha,\quad \tilde{N}=3^{-1/2}a\chi\sin\alpha\ ,$$

$$\Theta=2\pi ak_z,\quad \chi=(k_x^2+k_y^2)^{1/2}\ .$$

In these equations χ, which is the modulus of the vector $\boldsymbol{\chi}$ [Fig. 1(c)], determines how far we are removed from the HKH' edge in the k_x,k_y plane, and α is the angle between $\boldsymbol{\chi}$ and $\Gamma\mathbf{P}$, where P is any point in the HKH' edge [in Fig. 1(c), $P=K$]. The distance between neighbors in the graphitic plane is defined in Figs. 1(a) and 1(b).

The meaning of the various interaction parameters introduced is as follows.

(i) Interaction between nearest-neighbor atoms A-B,

$$\gamma_0=-\langle\phi(\mathbf{r}-\mathbf{r}_A)|H'|\phi(\mathbf{r}-\mathbf{r}_B)\rangle\ .$$

(ii) Interaction between adjacent atoms A-C,

$$\gamma_1=\langle\phi(\mathbf{r}-\mathbf{r}_A)|H'|\phi(\mathbf{r}-\mathbf{r}_C)\rangle\ .$$

(iii) Interaction between atoms $T=B$ or $T=D$ situated in second-neighbor planes,

TABLE I. Interaction parameters in eV.

Interaction parameter	A	B
γ_0	2.85	2.73
γ_1	0.30	0.32
γ_2	−0.02	−0.0186
γ_3	0.0	0.29
γ_4	0.0	0.15
γ_5	0.0	0.021
Δ	0.006	−0.017
E_F	−0.026	−0.0213

$$\gamma_2=2\langle\phi(\mathbf{r}-\mathbf{r}_T)\,|\,H'\,|\,\phi(\mathbf{r}-\mathbf{r}_T-\mathbf{a}_3)\rangle\ .$$

(iv) Interaction between atoms $T=B$ or $T=D$ in adjacent planes,

$$\gamma_3=\langle\phi(\mathbf{r}-\mathbf{r}_T)\,|\,H'\,|\,\phi(\mathbf{r}-\mathbf{r}_T)\rangle\ .$$

(v) Interaction between atoms $T=A$ or $T=B$ and $T'=D$ or $T'=C$ in adjacent planes,

$$\gamma_4=\langle\phi(\mathbf{r}-\mathbf{r}_T)\,|\,H'\,|\,\phi(\mathbf{r}-\mathbf{r}_{T'})\rangle\ .$$

(vi) Interaction between atoms $T=A$ or $T=C$ in second-neighbor planes,

$$\gamma_5=2\langle\phi(\mathbf{r}-\mathbf{r}_T)\,|\,H'\,|\,\phi(\mathbf{r}-\mathbf{r}_T-\mathbf{a}_3)\rangle\ .$$

(vii) Energy variation due to differences between sites A and B (the energy E_3 in point H of the first Brillouin zone is taken as a reference)

$$\Delta=\langle\phi(\mathbf{r}-\mathbf{r}_A)\,|\,H'\,|\,\phi(\mathbf{r}-\mathbf{r}_A)\rangle - \langle\phi(\mathbf{r}-\mathbf{r}_B)\,|\,H'\,|\,\phi(\mathbf{r}-\mathbf{r}_B)\rangle+\gamma_2+\gamma_5\ .$$

The determinant given in (5) has been solved analytically by several authors[14,15] for values of χ adjusted near the HKH' edge, without considering all the parameters. In our case we consider all the parameters and allow any value of χ. The interaction parameters γ_i are taken from the work of Dillon *et al.*[16] Structural details have been evaluated by Luiggi and Barreto[17] with each of Dillon's five sets of parameters. In this work we only utilize two sets of parameters. One set (the B set, Table I) is that which best reproduces the areas of the maximum orbits of electrons and holes reported by Dillon *et al.*[16] The other set (the A set, Table I) is that which is least successful in reproducing such areas. Table I shows both sets of parameters.

Figure 2 shows details of the band structure for both sets of parameters. The energy is plotted as a function of k_z on the KH edge (central part) and as a function of χ in the planes $k_z=0$ and $k_z=\pi/c$ along the direction $K-\Gamma$ and $H-A$, respectively. On the KH edge, both sets of parameters, A (dashed line) and B (solid line) indicate the existence of three bands labeled E_1, E_2, and E_3, the last being doubly degenerate. Outside the KH edge, band E_3 calculated from set A splits because of our base of wave functions $|\phi_n(n=1,2,3,4)\rangle$, but unfortunately they overlap with bands E_1 and E_2. The B set of parameters produces a complete splitting, thus giving four bands. In Fig. 2 is also indicated the location of the Fermi energy, $E_F\simeq-0.02$ eV, which at the KH edge cuts the bands E_2 and E_3, at the ΓK edge cuts the band E_3^+, and at the HA edge cuts the bands E_3^- and E_2 (for the bands evaluated with the set of parameters B) and the bands E_3 and E_2^- (for the bands evaluated with the set of parameters A). These cuts have a primary importance because they limit the type of current carrier which participates in the transport properties.

Constant-energy surfaces (CES), characterized by wave vector $\mathbf{k}_c(\chi,\alpha,k_z)$, are obtained from (5) by fixing E to a desired value. In our case the variables in the calculation have been α and χ to characterize the plane and $\Theta(k_z)$ for the perpendicular direction to the plane. CES are built by planes fixing k_z and α, and requiring a χ that satisfies (5). The value of χ is refined upon the CES for $|\mathbf{k}-\mathbf{k}_c|<10^{-10}$ through the inverse interpolation scheme of Aitken.[18]

Figures 3, 4, and 5 give some interesting details of these surfaces. In Fig. 3 we present tridimensional CES for the B set of parameters with $E=E_F$, $E>E_F$, and $E<E_F$. These surfaces show trigonal symmetry with planar satellites around the cutting point between the Fermi level E_F and the energy bands $E(k)$. Parameters γ_3 and γ_4 are responsible for the warping of the CES. This warping is

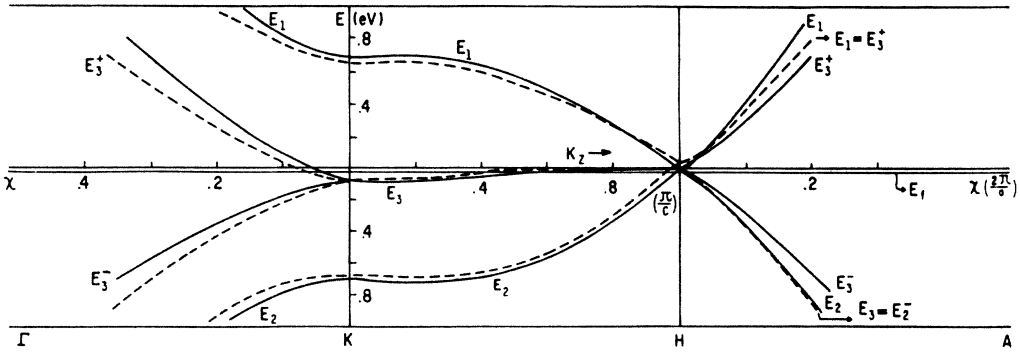

FIG. 2. Band structure of graphite.

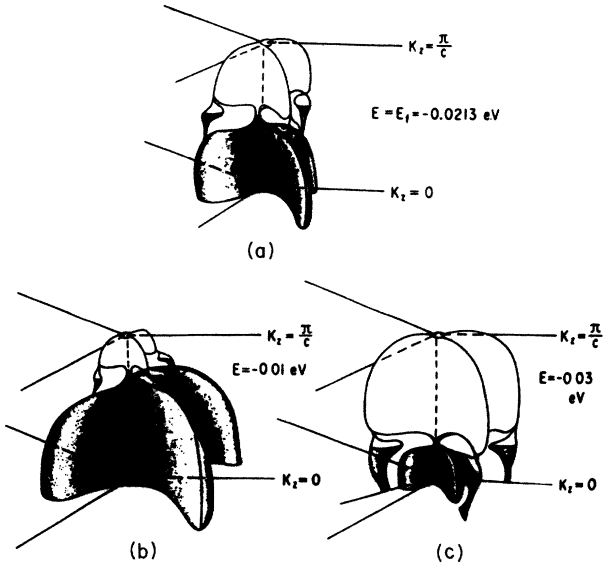

FIG. 3. Tridimensional constant-energy surfaces for different values of E. (a) $E=E_F=-0.0213$ eV. (b) $E=-0.01$ eV. (c) $E=-0.03$ eV.

necessary to explain galvanomagnetic properties in graphite.[19] The choice of $\gamma_2<0$, rather than $\gamma_2>0$ made by Ono and Sugihara, changes the distribution of holes and electrons around the center K and the top H of the HKH' edge. In Figs. 3(b) and 3(c) we show CES with energies above and below E_F, which constitutes a simplified view of what would happen if a donor ($E>E_F$) or acceptor ($E<E_F$) element were intercalated in graphite.[20] The A set of parameters leads to conical cylindrical surfaces which are rather different from the one given in Fig. 3. Those surfaces are used by the majority of researchers to calculate the transport properties.[8,10]

Figures 4(a) and 4(b) and 5(a) and 5(b) show the same effect of longitudinal and transverse cuts on CES for both sets of parameters. Longitudinal cuts correspond to different values of α and the transverse cuts are those for which $k_z=0$.

III. ELECTRON-PHONON INTERACTION

The phenomenological theory of Ono and Sugihara[9] considers the electron-phonon interaction in the rigid-ion model.[21] The evaluation of the matrix elements associated with that interaction is done between electron wave functions and hole wave functions in which the limits are deduced from band structure.

In our case, we do not introduce explicitly a deformation potential associated with the lattice vibration; instead, this effect is considered, assuming that the interaction between electrons and phonons displaces the atomic position by a distance $\delta\mathbf{r}$ from the static initial position of the lattice. The total wave function $|Y\rangle$ is then written as the product of the deformed electron wave function $|\Psi_k^d(\mathbf{r})\rangle$ and the phonon wave function $|\eta_p\rangle$. In this way, the Hamiltonian matrix evaluated with these wave functions is written

$$\langle Y|H|Y\rangle=\langle\eta_p\Psi_k^d(\mathbf{r})|H|\Psi_k^d(\mathbf{r})\eta_p\rangle\ . \tag{7}$$

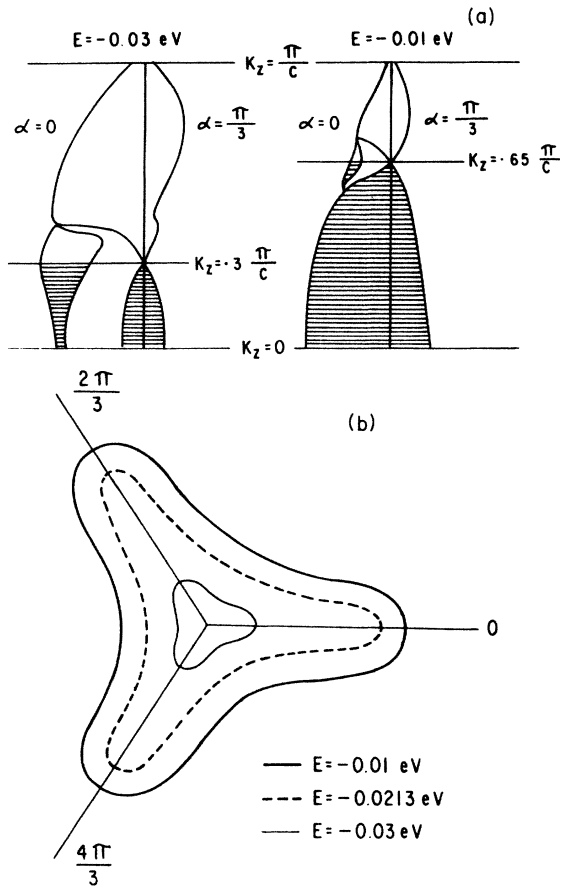

FIG. 4. Constant-energy surfaces for the set of parameters B. (a) Longitudinal cut for different values of E with $\alpha=0$ and $\alpha=\pi/3$. (b) Transverse cut for different values of E with $k_z=0$.

By analogy with the relation (1) the deformed wave function, $|\Psi_k^d(\mathbf{r})\rangle$ is written

$$|\Psi_k^d(\mathbf{r})\rangle=\sum_{t=1}\lambda_t|\phi_t^d\rangle\ , \tag{8}$$

where $|\phi_t^d(t=1,2,3,4)\rangle$ as in relation (2) is defined through the deformed wave functions $|\phi_t^d(t=A,B,C,D)\rangle$ centered in each of the atoms of the base, which are Bloch-type functions defined by

$$|\phi_t^d(\mathbf{r})\rangle=N^{-1/2}\sum_j\exp[i\mathbf{k}\cdot(\mathbf{r}_j+\delta\mathbf{r}_j)]\,|\phi(\mathbf{r}-\mathbf{r}_j)\rangle\ ; \tag{9}$$

the summation over j is for all the t atoms in the lattice.

Equation (9) shows the displacement $\delta\mathbf{r}_j$ of the jth atom due to lattice vibration. For small displacements, one can write (9) as

$$|\phi_t^d(\mathbf{r})\rangle=N^{-1/2}\sum_j[1+i\mathbf{k}\cdot\delta\mathbf{r}_j-\tfrac{1}{2}(\mathbf{k}\cdot\delta\mathbf{r}_j)^2]\times\exp(i\mathbf{k}\cdot\mathbf{r}_j)\,|\phi(\mathbf{r}-\mathbf{r}_j)\rangle\ . \tag{10}$$

The first term in (10) is associated with the static lattice; the second one contains the effect of the electron-phonon interaction. The third term is neglected for small displacements.

The overall effect of the electron-phonon interaction reduces simply to the evaluation of matrix elements, using the wave function defined in (10):

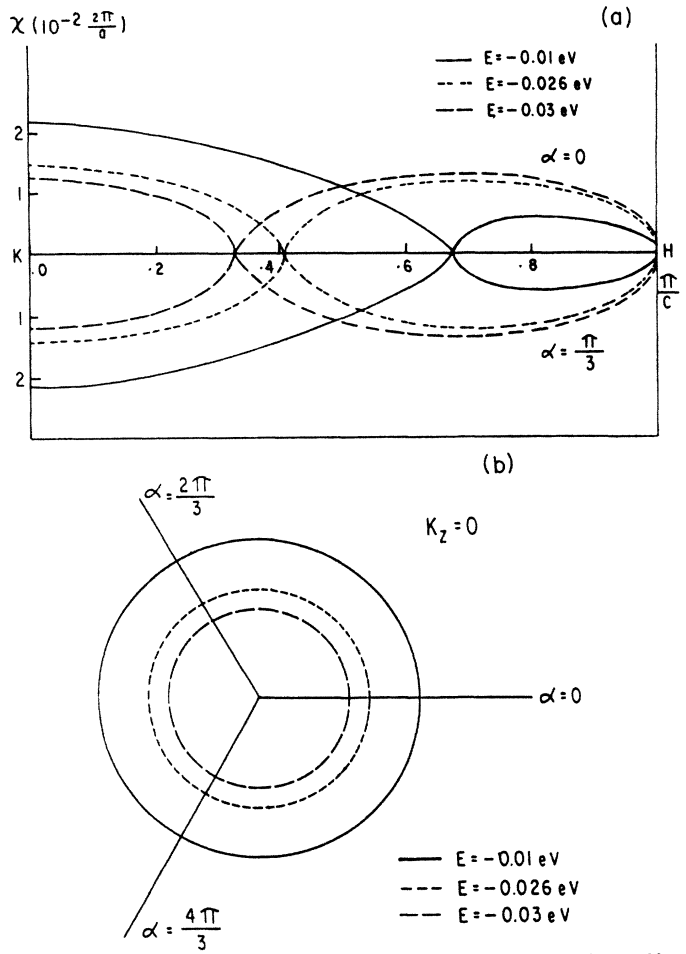

FIG. 5. Constant-energy surfaces for the set of parameters A. (a) Longitudinal cut for different values of E with $\alpha=0$ and $\alpha=\pi/3$. (b) Transverse cut for different values of E with $k_z=0$.

$$\langle \phi_i^d(\mathbf{r}) \mid H \mid \phi_h^d(\mathbf{r}) \rangle = N^{-1} \sum_{n,j} \exp[i(\mathbf{k}\cdot\mathbf{r}_j - \mathbf{k}\cdot\mathbf{r}_n)] \langle \phi(\mathbf{r}-\mathbf{r}_n) \mid H \mid \phi(\mathbf{r}-\mathbf{r}_j) \rangle + N^{-1} \sum_{n,j} i(\mathbf{k}\cdot\delta\mathbf{r}_j - \mathbf{k}\cdot\delta\mathbf{r}_n) \exp[i(\mathbf{k}\cdot\mathbf{r}_j - \mathbf{k}\cdot\mathbf{r}_n)] \langle \phi(\mathbf{r}-\mathbf{r}_n \mid H \mid \phi(\mathbf{r}-\mathbf{r}_j) \rangle \ . \tag{11}$$

Taking $\mathbf{r}_n - \mathbf{r}_j = \mathbf{T}_{nj}$, where $\mathbf{T}_{nj}$ is a translation vector, (11) can be rewritten as

$$\langle \phi_i^d(\mathbf{r}) \mid H \mid \phi_h^d(\mathbf{r}) \rangle = \sum_n \exp(-i\mathbf{k}\cdot\mathbf{T}_{nj}) \langle \phi(\mathbf{r}-\mathbf{r}_n) \mid H \mid \phi(\mathbf{r}-\mathbf{r}_j) \rangle + \sum_n i(\mathbf{k}-\mathbf{k}')\cdot\delta\mathbf{r}_n \langle \phi(\mathbf{r}-\mathbf{r}_n) \mid H \mid \phi(\mathbf{r}-\mathbf{r}_j) \rangle \exp(-i\mathbf{k}\cdot\mathbf{T}_{nj}) \ , \tag{12}$$

in which we have centered on the jth atom. Notice that j ($j = A,B,C,D$) is fixed, whereas n runs through all the atoms A, B, C, and D. The first term in (13) is the same mentioned above for the static lattice. The deformation has the effect of introducing $\delta\mathbf{r}_n$ as a phonon operator which acts upon the phonon part $\mid \eta_p \rangle$ in (7).

In usual notation,[21] $\delta\mathbf{r}_n$ is written as

$$\delta\mathbf{r}_n = \sum_{q,p} \left[\frac{\hbar}{2NM\omega_p(q)} \right]^{1/2} \exp(i\mathbf{q}_p\cdot\mathbf{r}_n)[a^+(-q_p) + a^-(q_p)]e_p(\mathbf{q}) \ , \tag{13}$$

where $\mathbf{q}$ is the phonon wave vector, p fixes the type of vibrational mode, $\mathbf{e}$ is the phonon polarization vector, and a^+ and a^- are the creation and annihilation phonon operators, which lead to matrix elements different from zero if the wave functions $\mid \eta_p \rangle$, upon which they operate, represent phonon states whose occupation numbers differ by one phonon.

After some algebraic operations, relation (7) can be written for normal processes as

$$\langle H \mid H \mid Y \rangle = -i \langle \Psi_{\mathbf{k}} \mid H \mid \Psi_{\mathbf{k}'} \rangle (\mathbf{k}-\mathbf{k}') \cdot \sum_{p,\mathbf{q}} \left[\frac{\hbar n_{\mathbf{q},p}}{2NM\omega_p(\mathbf{q})} \right]^{1/2} \mathbf{e}_p(\mathbf{q}) \ , \tag{14}$$

where $n_{q,p}$ is the number of phonons defined by Bose statistics.

Relation (14) defines the matrix elements of the electron-phonon interaction as the product of the matrix elements of the static lattice (evaluated in the last section) multiplied by a factor which is due to the phononic effects; this relation is more general than that referred to by Ziman[21] for the group of models of rigid ions, deformable ions, and deformation potentials. It also has the advantage of introducing no less phenomenologic parameters than those introduced in the SWMc model of the band structure. Considering that only acoustic phonons participate in the dispersion, (14) transforms to

$$\langle Y \mid H \mid Y \rangle = -i \langle \Psi_{\mathbf{k}} \mid H \mid \Psi_{\mathbf{k}'} \rangle \left[q_{\parallel} \left[\frac{\hbar n_{q_{\parallel}}}{2NM\omega_{q_{\parallel}}} \right]^{1/2} + q_{\perp} \left[\frac{\hbar n_{q_{\perp}}}{2NM\omega_{q_{\perp}}} \right]^{1/2} \right], \tag{15}$$

where

$$n_{q_i} = \left[\exp\left[\frac{\hbar\omega(q_i)}{KT} \right] - 1 \right]^{-1} \quad \text{with } i = \parallel \text{ or } \perp .$$

Each of the terms in the matrix elements allows us to introduce the parallel or perpendicular characteristics associated with these vibrational modes.

IV. RELAXATION TIME

The inverse of the relaxation time is defined by

$$\tau^{-1} = \int P_{\mathbf{k},\mathbf{k}'}(1-\cos\theta_{\mathbf{k},\mathbf{k}'})ds' , \tag{16}$$

where $P_{k,k'}$ defines the transition probability between electronic states $\mid k \rangle$ and $\mid k' \rangle$. The factor $(1-\cos\theta_{\mathbf{k},\mathbf{k}'})$ characterizes momentum transfer in the process for incident $\mid k \rangle$ and $\mid k' \rangle$ electron wave vectors, θ being the angle between them.

$P_{\mathbf{k},\mathbf{k}'}$ is written usually as

$$P_{\mathbf{k},\mathbf{k}'} = \frac{2\pi}{\hbar} \mid \langle Y \mid H \mid Y \rangle \mid^2 \delta(E(\mathbf{k}')-E(\mathbf{k})\pm\hbar\omega_{\mathbf{q}}) . \tag{17}$$

Taking into account that vibrational modes are divided into two groups which are parallel ($q_{\parallel}$) and perpendicular ($q_{\perp}$) to the plane,[6] we introduce in (16) the transition probabilities associated with both modes; that is, we define

$$\begin{aligned} \tau_{\parallel}^{-1} &= \int P_{\parallel}(1-\cos\theta)ds' , \\ \tau_{\perp}^{-1} &= \int P_{\perp}(1-\cos\theta)ds' . \end{aligned} \tag{18}$$

Both relaxation times are evaluated with the help of the following relations in cylindrical coordinates:

$$\begin{aligned} &\mid k \rangle = \mid \chi\cos\alpha, \chi\sin\alpha, k_z \rangle , \\ &\mid k' \rangle = \mid \chi'\cos\alpha', \chi'\sin\alpha', k_z \rangle , \\ &\mid q \rangle = \mid \chi'\cos\alpha' - \chi\cos\alpha, \chi'\sin\alpha' - \chi\sin\alpha, k_z' - k_z \rangle , \\ &\cos\theta = [k_z k_z' + \chi\chi'(\cos\alpha\cos\alpha' + \sin\alpha\sin\alpha')]/kk' , \\ &q^2 = \chi'^2 + \chi^2 - 2\chi\chi'(\cos\alpha\cos\alpha' + \sin\alpha\sin\alpha') . \end{aligned} \tag{19}$$

The evaluation of (16) is done over the CES, such that the area element ds' is taken on each of those surfaces. The numerical calculus is easier if our surface is projected over a cylindrical surface, so that

$$ds' = \chi' \, d\alpha' \, dk_z' \left[\frac{\nabla_{\mathbf{k}} E}{\mid \nabla_{\mathbf{k}} E \mid} \cdot \chi_{\alpha'} \right] , \tag{20}$$

where $\chi_{\alpha'} = (\cos\alpha', \sin\alpha')$ is a unitary vector normal to the cylindrical surface and the ratio of energetic gradients is a unitary vector normal to the CES.

Considering the elastic scattering approximation in which phonon energies are considered insignificant with respect to electronic energies, Eq. (18) can be written, after using (13), (15), and (17), as

$$\tau_{\parallel}^{-1} = \frac{3\Omega}{M\pi^2} \int \frac{q_{\parallel}^2 n_{\parallel}(1-\cos\theta) \mid \langle \Psi_{\mathbf{k}} \mid H \mid \Psi_{\mathbf{k}'} \rangle \mid^2}{\omega_{\parallel} \mid \nabla_{\mathbf{k}'} E \mid} ds' , \tag{18'}$$

$$\tau_{\perp}^{-1} = \frac{3\Omega}{M\pi^2} \int \frac{q_{\perp}^2 n_{\perp}(1-\cos\theta) \mid \langle \Psi_{\mathbf{k}} \mid H \mid \Psi_{\mathbf{k}'} \rangle \mid^2}{\omega_{\perp} \mid \nabla_{\mathbf{k}'} E \mid} ds' . \tag{18''}$$

Phonon occupation $n_{\parallel}$ and $n_{\perp}$ as well as matrix elements are taken in the same way as in the preceding section.

Each of the integrals is evaluated for a CES with k_z varying between points K and H of the first Brillouin zone, and owing to trigonal symmetry, α scans $\frac{1}{6}$ of each plane in which k_z is constant. The role of holes and electrons in this formulation is controlled by the k_z parameter (Figs. 3, 4, and 5) because there exists a k_z value, that depends on the energy, for which the orbits for electrons and hole touch each other and have a minimum area.

The value $\omega(q)$ has been taken directly from neutron inelastic scattering measurements of Nicklow *et al.*[12] for pyrolitic graphite. We have also adjusted modes 1 and 2 of Komatsu's relations,[6] which corresponded to our parallel and perpendicular modes, to the longitudinal acoustic branch of Nicklow *et al.*,[12] obtaining the following dispersion relation:

$$\omega = \omega_1 \sin(aq_{\parallel}/4), \quad \omega = \omega_2 \sin(cq_{\perp}/2) , \tag{21}$$

with $\omega_1 = 10^{12} s^{-1}$ and $\omega_2 = 2\times 10^{11} s^{-1}$.

V. ELECTRONIC WAVE-FUNCTION COEFFICIENTS

The relations (18') and (18'') are completely defined when we know the electronic wave-function coefficients introduced in (1). In their evaluation we recall that the secular equation (4) is a homogeneous system of equations

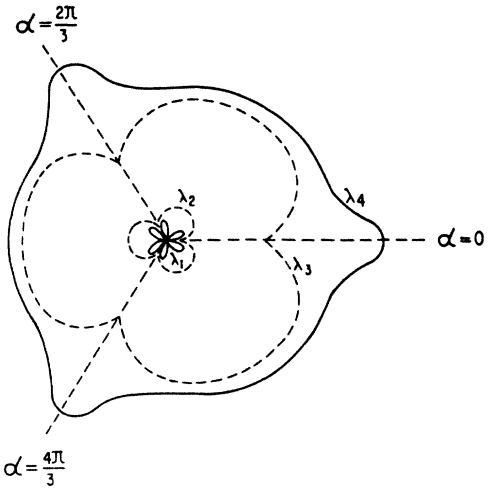

FIG. 6. Electron wave-function coefficients λ evaluated on the Fermi surface. The values of λ_1 and λ_2 are exaggerated.

in those coefficients. Also we suppose that the wave functions associated with each atom do not overlap $\langle\Psi|\Psi\rangle=\sum\lambda_i\lambda_j^*=1$, so that we get an overdetermined system of equations of five equations and four unknowns.

The overdetermination presupposes an infinite number of solutions. But in our case, on evaluating these coefficients for CES, we get unique solutions for λ_i which are independent of the selected system for their calculation.

Figure 6 gives the form of the coefficients for the set of parameters B, with $E=E_F$ in the plane $k_z=0$. As can be seen, the coefficients have the trigonal symmetry of the Fermi surface. Coefficients λ_3 and λ_4, associated with atoms B and D (situated in different planes) are ten times larger than λ_1 and λ_2 associated with the atomic combination A,C. For increasing values of k_z this correlation between coefficients changes, passing to weigh more the λ_1 and λ_2 coefficients. Note that this consideration must have some influence on the magnitude of the transport coefficients and therefore we must take care when we consider graphite as a two-dimensional semimetal instead of a three-dimensional one, as really it is.

VI. DISCUSSION

The results which follow have been obtained by the numerical evaluation of relations (18′) and (18″), using a Cyber 171 computer. The temperature is defined through use of $n_{||}$ and $n_\perp$ and is maintained fixed for each calculation on the CES, which were determined for fixed values of energy in the vicinity of the Fermi energy.

A. Electron and hole contributions

In Fig. 7 the relaxation time $\tau=(\tau_{||}^{-1}+\tau_\perp^{-1})^{-1}$ at the KH edge is plotted as a function of k_z. For this calculation we selected the CES $E=E_F$ and used $\alpha=0$ and $\alpha=\pi/3$ to emphasize the details of the Fermi-surface anisotropy. Temperature was fixed at 25 and 300 K and the set of interaction parameters A defined in Table I was used.

This graph shows an increasing τ in the electron zone

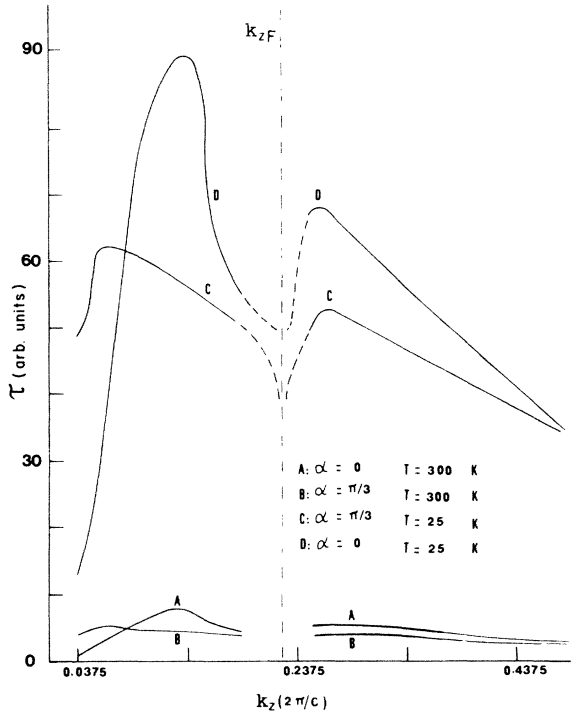

FIG. 7. Relaxation time in arbitrary units as a function of k_z for $T=25$ and 300 K and for $\alpha=0$ and $\pi/3$.

[stippled region in Fig. 3(a)] from $k_z=0$ to an intermediate value between the K point and the k_{zf} point. After that, τ decreases to a minimum in the vicinity of the k_{zf} point. In the hole zone a similar behavior, although less pronounced, is observed. The results are, in general, in agreement with those reported by Ono and Sugihara,[19] where their selection of $\gamma_2>0$ exchanges, with respect to this work, the results for electrons and holes. Note that for values of k_z where χ is multivalued [region of the Fermi surface where the satellites appear, Fig. 3(a)], we show with dashed lines at $T=25$ K the dependence of τ on k_z.

The Fermi-surface anisotropy appears for the values of $\alpha=0$ and $\alpha=\pi/3$, showing a tendency towards isotropy at the H end of the first Brillouin zone. The minimum value of τ at the K point, where the electronic orbit is maximum (Figs. 3 and 4) can be understood if we take into account that τ is inversely proportional to the carrier density.[10]

The behavior in the vicinity of k_{zf}, indicated in the figure for $T=25$ K, is due to the fact that for $\alpha=0$ there are well-defined orbits, while at that point for $\alpha=\pi/3$ there is a minimum orbit, defining a value $\nabla_{\mathbf{k}}E$ some orders of magnitude smaller than in other orbits. That leads to the decrease in τ. Finally, the effect of the temperature is that which is expected, in other words, τ is larger for higher temperatures.

B. Parallel and normal relaxation times

In Fig. 8 we show the evolution of the parallel relaxation time [Fig. 8(a)] and the evolution of the normal relaxation time [Fig. 8(b)] both as functions of energy; all that for our best set of parameters (set B), in the temperature range between 25 and 300 K for both relaxation-time

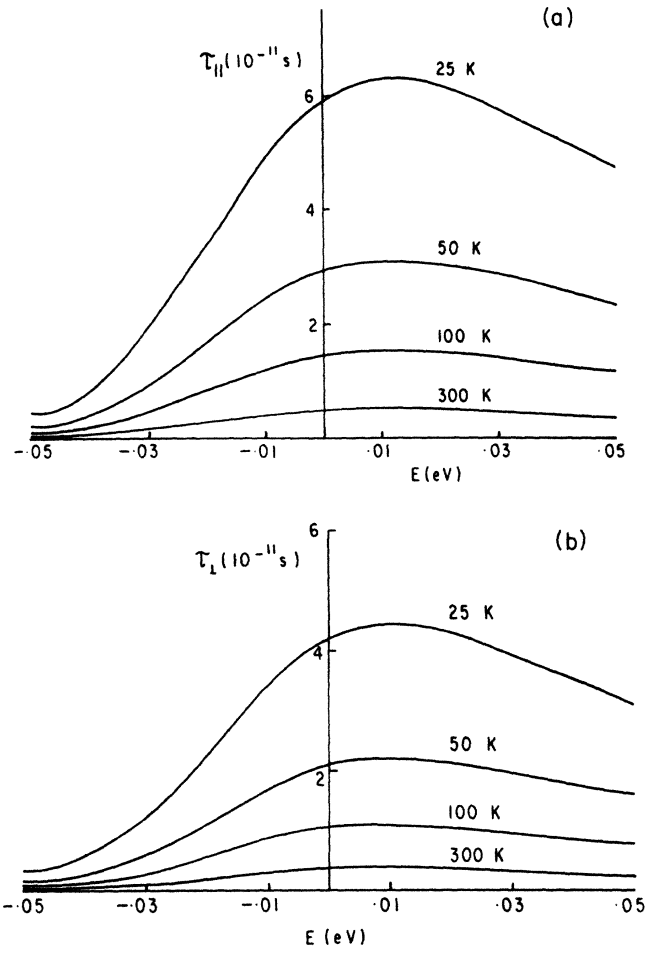

FIG. 8. Relaxation time as a function of energy for different temperatures for the set of parameters B. (a) Parallel relaxation time versus energy. (b) Perpendicular relaxation time versus energy.

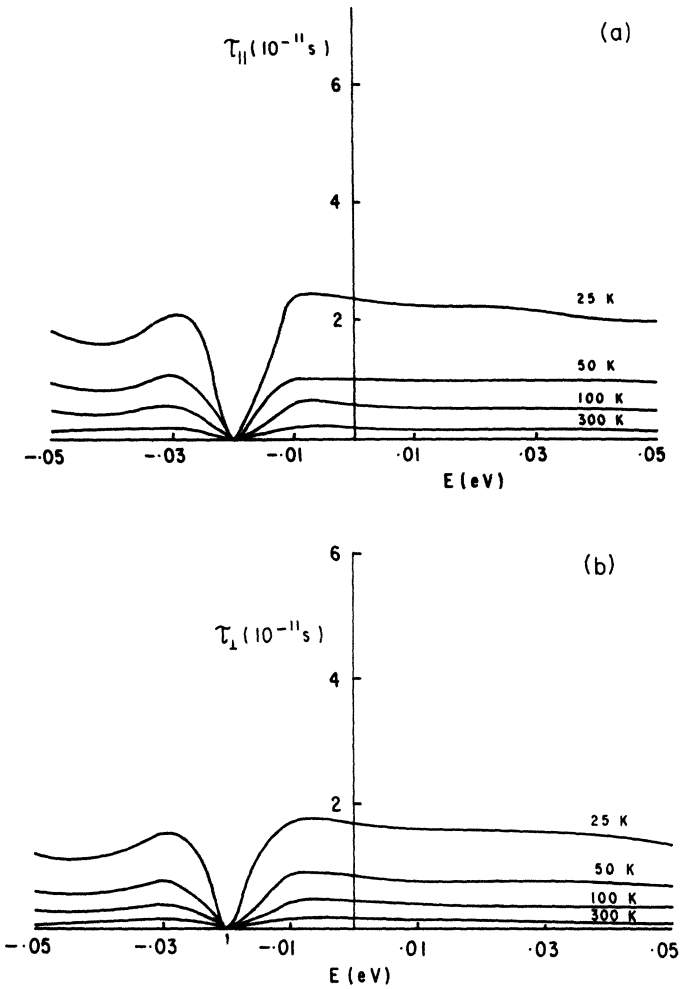

FIG. 9. Relaxation time as a function of energy for different temperatures for the set of parameters A. (a) Parallel relaxation time versus energy. (b) Perpendicular relaxation time versus energy.

behaviors. In the energy range under study there is an increase of τ, a minimum, and a decrease of τ. For energies below E_F the parallel relaxation time varies between 5×10^{-13} s at $T=300$ K and 5×10^{-12} s at $T=25$ K, whereas the perpendicular relaxation time varies between 10^{-13} and 3×10^{-12} s. For $E\simeq0.01$ eV, both times reach their maximum values: $\tau_{\|}=6\times10^{-11}$ s and $\tau_{\perp}=4.2\times10^{-11}$ s at 25 K. For energies greater than E_F the relaxation times diminish and tend to be constant. The effect of decreasing temperature is to increase τ. Our results are encouraging because they agree qualitatively with the ones reported by Ono and Sugihara[9] and Olsen.[10] It is important to mention that our calculation has not been adjusted to reproduce experimental transport coefficients.

When the set of parameters A is used to calculate $\tau_{\|}$ and $\tau_{\perp}$ [Figs. 9(a) and 9(b)], we get a behavior of τ, as a function of energy, slightly different from the one obtained before; nevertheless, both $\tau_{\|}$ and $\tau_{\perp}$ have a good order of magnitude (10^{-13}–10^{-11} s) and a reasonable behavior with temperature. In this calculation we have chosen and integration increment in k_z such that the minimum orbit on the CES is avoided [Fig. 5(a)]. In the case where the set of parameters B was used, the CES showed such orbits on the HKH' edge but the presence of satellites introduced through the γ_3 and γ_4 parameters [Figs. 3(a), 3(b), and 3(c)] with orbits of areas well defined, avoided any computational complication in the evaluation of (18′) and (18″).

Presently, following our formulation, we are studying the transport coefficients of crystalline graphite, and we have gotten satisfactory results for the electric conductivity on the graphitic plane. The best agreement is for $T=300$ K, where we know that the relation (16) is good enough. For the resistivity normal to the graphitic plane, we have gotten a metallic dependence with temperature.[17]

We also note here that, inasmuch as the effect of intercalation will produce little structural change in the planar characteristics of graphite, the formulation for the parallel relaxation time reported here should also apply, at least in first approximation, to intercalated graphite by donors ($E>E_F$) or by acceptors ($E<E_F$). A discussion of this topic is is given by Pietronero and co-workers.[22,23] In the

search for a model adequate to explain the electrical properties of intercalants, it is necessary to consider the effects of charge transfer between the carbon atoms and those of the intercalant,[24] as well as their respective ionization potentials. The aim of the search is to achieve the proper variation of the perpendicular properties of intercalants (relaxation time, conductivity, etc.) with respect to those of crystalline graphite.

In a future paper we extend the details of the formulation reported here, with respect to band structure, Fermi surfaces, and relaxation times, to the study of the intercalant KC_8. We obtain a value of $\sigma_{\|}/\sigma_{\perp}$ of approximately 90 and a value of $\sigma_{\|}$, in complete agreement with that reported by Vogel *et al.*[25]

To conclude, we have formulated a relatively simple way of determining the relaxation time in graphite which can be extended to apply to intercalated graphite. The electron-phonon interaction is the dominant scattering mechanism and its matrix elements introduce independently the phononic contributions and the details associated with the static lattice of graphite. We have verified that the interaction parameters that select the Fermi surface affect both the magnitude and the form of dependence of τ on energy. Our results are encouraging because they are in agreement with the general results reported in the literature, and their use in the evaluation of the electric resistivity in graphite and intercalated graphite predicts magnitudes according to the measured ones.

ACKNOWLEDGMENTS

Thanks are due to the computer center of the Universidad de Oriente for providing extended computation time. We appreciate very much the advice of Dr. J. L. Gil Zambrano, Dr. J. Franco, and Dr. L. Acuña for revising the manuscript. Financial support from the Consejo Nacional de Investigaciones Cientificas y Tecnológicas (CONICIT) and from the Consejo de Investigaciones de la Universidad de Oriente is gratefully acknowledged.

[1]J. McClure, Phys. Rev. **108**, 612 (1957).
[2]W. Wegener and L. Fritsche, Phys. Status Solidi B **78**, 585 (1976).
[3]R. Tatar and S. Rabii, Phys. Rev. B **25**, 4126 (1982).
[4]J. Slonczewski and P. Weiss, Phys. Rev. **109**, 272 (1958).
[5]L. Johnson and G. Dresselhuas, Phys. Rev. B **7**, 2275 (1973).
[6]K. Komatsu, J. Phys. Chem. Solids **25**, 707 (1964).
[7]P. Wallace, Phys. Rev. **71**, 622 (1947).
[8]K. Sugihara and H. Sato, J. Phys. Soc. Jpn. **18**, 322 (1963).
[9]S. Ono and K. Sugihara, J. Phys. Soc. Jpn. **21**, 861 (1966).
[10]L. Olsen, Phys. Rev. **6**, 4836 (1972).
[11]R. Dillon and I. Spain, J. Phys. Chem. Solids **39**, 923 (1978).
[12]K. Niclow, N. Wakabayashi, and H. Smith, Phys. Rev. **5**, 4951 (1972).
[13]F. Cotton, *Chemical Application of Group Theory* (Wiley Interscience, New York, 1971).
[14]H. Nagayoshi, K. Nakao, Y. Uemura, J. Phys. Soc. Jpn. **41**, 1480 (1976).
[15]A. Maaroufi, S. Flandrois, C. Coulon, and J. Rouillon, J. Phys. Chem. Solids **43**, 1103 (1982).
[16]R. Dillon, I. Spain, and J. McClure, J. Phys. Chem. Solids **38**, 635 (1977).
[17]N. Luiggi and W. Barreto, Acta Cient. Venez. **207**, Suppl. 1, 35 (1984).
[18]N. Kopchenova and I. Maron, *Computational Mathematics* (Ed. MIR, Moscow, 1981).
[19]S. Ono and K. Sugihara, J. Phys. Soc. Jpn. **24**, 818 (1968).
[20]U. Gubler, J. Krieg, P. Pfluger, and J. Güntherodt, in *Physics of Intercalation Compounds*, Vol. 38 of *Springer Series in Solid State Physics*, edited by L. Pietronero and E. Tosatti (Springer, Berlin, 1981), p. 68.
[21]J. Ziman, *Electrons and Phonons* (Oxford University Press, London, 1979).
[22]L. Pietronero, S. Strässler, H. Zeller, and M. Rice, Phys. Rev. B **22**, 904 (1980).
[23]L. Pietronero and S. Strässler, J. Phys. Soc. Jpn. A Suppl. **49**, 895 (1980).
[24]T. Inoshita, K. Nakao, and H. Kamimura, J. Phys. Soc. Jpn. **43**, 1237 (1977).
[25]F. Vogel, P. Wachnik, and L. Pendrys, in *Physics of Intercalation Compounds*, Vol. 38 of *Springer Series in Solid State Physics*, edited by L. Pietronero and E. Tosatti (Springer, Berlin, 1981), p. 288.